Theory and experimental program for

p-B^{11} Fusion with the Dense Plasma Focus

Eric J. Lerner, S. Krupakar Murali, and A. Haboub
Lawrenceville Plasma Physics Inc.
128 Lincoln Blvd.
Middlesex, NJ 08846-1022, USA
Tel: (732) 356 5900, Fax: (732) 377 0381, E-mail: eric@LPPhysics.com

Abstract: Lawrenceville Plasma Physics Inc. has initiated a two-year-long experimental project to test the scientific feasibility of achieving controlled fusion using the dense plasma focus (DPF) device with hydrogen-boron (p-B^{11}) fuel. The goals of the experiment are: first, to confirm the achievement of high ion and electron energies observed in previous experiments from 2001; second, to greatly increase the efficiency of energy transfer into the plasmoid where the fusion reactions take place; third, to achieve the high magnetic fields (>1 GG) needed for the quantum magnetic field effect, which will reduce cooling of the plasma by x-ray emission; and finally, to use p-B^{11} fuel to demonstrate net energy gain. The experiments are being conducted with a newly constructed dense plasma focus in Middlesex, NJ which is expected to generate peak currents in excess of 2 MA. Some preliminary results are reported.

Key words: *Dense plasma focus, quantum magnetic field effect, nuclear fusion, aneutronic fusion*

1. Introduction

Controlled nuclear fusion using hydrogen-Boron-11 (p-$B^{11)}$ fuel would constitute a transformative source of electricity with major advantages over any other known source of energy. No neutrons are produced in this reaction, $p + B^{11} \rightarrow 3\ He^4$, and the released energy is carried only by charged particles. This makes possible the direct conversion of the kinetic energy of these charged particles into electricity without going through the inherently expensive process of using heat to produce steam to run a turbine and generator. It thus opens up the possibly of drastically reducing the cost of electricity generation. [1-3]

While a secondary reaction, $He^4+B^{11} \rightarrow N^{14} + n$, does produce neutrons, they carry only 0.2% of the fusion energy and are low-energy neutrons, which are easily shielded. Thus this fuel makes conceivable the design of a generator that produces insignificant amounts of induced radioactivity, and no radioactive waste. These characteristics give p-B^{11} very significant operational advantages over deuterium-tritium (DT) fuel.

However, p-B^{11} presents two major technical challenges that have discouraged funding and research. First, the reaction requires average ion energies above 100 keV, considerably higher than the 40 keV envisioned for DT fuel, and the requirement for plasma density-confinement time product ($n\tau$) is also a factor of 45 times higher for net energy production. Second, the higher atomic charge of boron ions leads to the production of far greater amounts of X-ray energy than DT, and the emission of such X-ray energy cools the plasma, making plasma heating more difficult. We have taken steps to show how both of these technical challenges can be overcome using the DPF.

2. Dense Plasma Focus (DPF)

The DPF is a compact and simple device first developed in the 1960s by N. V. Filippov in the USSR and by J. W. Mather in the USA and has been studied by dozens of groups over the last 45 years, resulting a large and rich literature. It consists of two concentric cylindrical electrodes enclosed in a vacuum chamber. The chamber is evacuated to low pressure and then backfilled to several torr with the fuel gas. A pulse of electricity with a rise time of 0.2-10 μs from a capacitor bank is discharged across the electrodes during operation. [4] In operation, the capacitors discharge in a several-microsecond pulse, the gas is ionized and a current sheath, consisting of pinched current filaments, forms and runs down the electrodes. When the sheath reaches the end of the inner electrode (the anode), the filaments pinch together, forming dense, magnetically-confined, hot spots or plasmoids.[5-6] The plasmoids emit X-rays with energy from several keV to over 100 keV. X-ray pinhole images have demonstrated that the plasmoids are tiny, with radii of tens of microns or less [7-11]. The plasmoids have densities in the range of 10^{20} - 10^{21} /cm^{3}. These densities have been measured by a number of independent methods including heavy ion and secondary product fusion[12-13], CO_2 laser scattering[14], and x-ray line intensities[15].These plasmoids emit intense beams of accelerated ions and electrons[16-19]. Fusion neutrons are emitted from the device in large quantities (up to 10^{13}) per shot.

The role of the plasmoids in producing the fusion neutrons and the physical processes involved in their formation and maintenance has been hotly debated among DPF researchers for decades. The model that best fits all the existing data makes the role of the plasmoids central to neutron production. This model, initially developed by Bostick and Nardi[4], and confirmed by observations of several groups over three decades, was elaborated into a more quantitative theory by the present author[20-24]. In this model, the electron beam transfers part of its energy to the plasmoid electrons, which generate X-rays through collisions with nuclei. Through a plasma instability (probably ion-acoustic), the electrons then transfer part of their energy to the ions, with a typical delay (in our experiments) of ~10 ns. Ion collisions, generating fusion reactions and neutrons, then occur [24]. When the ion and electron beams have exhausted the magnetic energy that confines the plasmoid, and partially or wholly evacuated the particles in the plasmoid, the fusion reactions end.

The DPF routinely produces hard X-rays and gamma rays indicating the presence of bremsstrahlung radiation from high-energy electrons colliding with nuclei[21]. Together with independent evidence, this indicated that the hot spots contained ions and electrons at very high energies in the range of interest for advanced fuel fusion [6, 14, 15, 22-24].

The Bostick-Nardi model detailed in [4] describes the DPF as operating by exploiting a series of natural instabilities in the plasma, with each instability further concentrating the plasma and the magnetic field produced by the currents running through the plasma. In the past few decades, substantial advances have occurred in understanding the basic physics of such instabilities through experiments and observations of space plasma.

In the first instability, the current sheath moving through the plasma between electrodes breaks up into an array of filaments, increasing the density of the plasma and magnetic field strength by a factor of 10-20. The filamentary current sheath, driven by the interaction of its own currents and magnetic field, travels down to the end of the inner hollow electrode, where the filaments converge into a single central pinch region, further concentrating both plasma and magnetic fields. A third instability then kinks the single central

filament like an over-twisted phone cord, forming a plasmoid, an extremely dense, magnetically self-confined ball of plasma only tens of microns across. By this time, the density and magnetic fields of the plasma in this small region are tens of thousands of times larger than those present at the start of the process, and a substantial fraction of the energy fed into the device is contained in the plasmoid. A fourth instability causes the magnetic fields at the center of plasmoid to decrease, and these changing magnetic fields induce an electric field, which generates a beam of electrons in one direction and a beam of ions in the other. The electron beam heats the plasmoid electrons which in turn heat the ions, thus igniting fusion reactions. The energy is released in the ion and electron beams and in a burst of X-ray energy from the heated electrons in the plasmoid.

In addition to its very small size, simplicity, and ability to utilize the inherent plasma instabilities (rather than suppressing them), the DPF also has the advantage that the plasmoid is extremely dense. Such a dense plasmoid requires that the ions be confined for only a few thousand orbits, in contrast to the millions of orbits required in tokomaks or most other fusion devices. Thus the high stability of such devices is not required in the DPF, only meta-stability.

3. Quantum Magnetic Field (QMF) Effect

Lerner theoretically showed [22] that the problem of high X-ray emission with p-B^{11}could be mitigated through the use of the QMF effect. This effect, first pointed out in the 1970's, [25] and studied in the case of neutron stars [26], involves the reduction of energy transfer from ions to electrons in the presence of a strong magnetic field. To apply the magnetic effect to the DPF plasmoids, which are force-free configurations, we first note that small-angle momentum transfer parallel to the field can be neglected in these plasmoids, since the ion velocity lies very close to the local magnetic field direction, and $\Delta p_{\|}/\Delta p_{\perp}$ ~$\sin^2\theta$, where θ is the angle between the ion velocity and the B field direction[22].

In a strong magnetic field, since angular momentum is quantized in units of ħ, electrons can have only discrete energy levels, termed Landau levels (ignoring motion parallel to the magnetic field):

$$E_b = \left(n+\tfrac{1}{2}\right)\frac{e\hbar B}{mc} = \left(n+\tfrac{1}{2}\right)\cdot 11.6eV\cdot B(GG) \quad \textbf{(1)}$$

Since maximum momentum transfer is mv, where v is relative velocity, for $mv^2/2 < E_b$ almost no excitation of electrons to the next Landau level can occur, so very little energy can be transferred to the electrons in such collisions. Again ignoring the electron's own motion along the field lines, such a condition will occur when ion energy

$$E_i < \left(\frac{M}{m}\right)E_b \quad \textbf{(2)}$$

For E_i =300keV, this implies B>14GG for p, B>3.5GG for α , and B>1.3GG for ^{11}B. As will be shown below, such field strengths should be attainable with the DPF.

As calculated[22], for $T=T_i/E_b(M/m)<1$, the coulomb logarithm can drop as low as 0.5 for the heating of electrons by ions, which can only heat electrons that are moving slower than the ions. For the heating of the ions by the much faster thermal electrons, with $T_e>>1$, quantum effects can be ignored and the coulomb logarithm is simply $ln(2T_e)$. As a result, the ratio of these two coulomb logarithm terms can be as high as 20, which results in a similar value for T_i/T_e. This results in a reduction of x-ray emission by as much as a factor of four.

We have performed 0-D simulations of the plasmoid which include this QMF effect [24] which show that in this case fusion power can potentially exceed Bremsstrahlung emission by as much as a factor of 2, allowing ignition of the fuel

and an 80% burn-up of the fuel in the plasmoid. While not fully realistic, the simulation is adequate to show the impact of the magnetic effect and the possibility for high fusion yields in which the energy emitted in the form of x-rays and ion beams exceeds the total energy input to the plasma by about a factor of two. Of course, this by no means guarantees that direct energy conversion efficiency will be high enough for a practical generator, but it does indicate that this is at least conceivable, and worth investigating experimentally.

The simulation, by its zero-dimensional character, assumes that the plasma in the plasmoid is homogenous. In addition the simulation assumes Maxwellian distributions for the electrons, and hydrogen and boron ions. Helium ions, produced by the fusion reaction, are assumed to cool to a Maxwellian distribution, but the fusion alpha particles are treated separately, as they are slowed by the plasma. In accordance with observation, it is assumed that the ions are all fully ionized.

This simulation also assumes that the plasma radius contracts during compression and then remains stable. Thus it is assumed that as fusion energy is released, countervailing forces prevent the rapid expansion of the plasmoid.

There are good experimental reasons for believing that this is as at least roughly the case, as we explain here. Half the fusion energy released in DD reactions is deposited in the plasmoids by the d+d $\rightarrow$ p+t reaction. In the plasmoids measured in, for example, Lerner[22], the additional pressure from this deposited energy would disassemble the plasmoids is a few ps, thousands of times shorter than their observed lifetime of tens of ns, unless the pressure was balanced by an increase in confining forces.

We intend to discuss the role played by centrifugal stabilization in the long lifetime of the plasmoids in a future paper.

4. Conditions in DPF plasmoids

To see what the consequences of the QMF effect are for DPF functioning, we use a theoretical model of DPF functioning that can predict conditions in the plasmoid, given initial conditions of the device. As described by Lerner, [20,22-23]and Lerner and Peratt, [21] the DPF process can be described quantitatively using only a few basic assumptions. First, we assume that the magnetic energy of the field is conserved during the formation of the plasmoid, and that in a well-formed pinch, all the energy present in the field at the time of the pinch is trapped in the plasmoid. Second, plasma instability theory, as detailed in [20], shows that for optimal filament formation in the plasma chamber the following condition has to be satisfied.

$$\omega_{ce} = \omega_{pi} \qquad \textbf{(3)}$$

where ω_{ce} is electron gyrofrequency and ω_{pi} is ion plasma frequency.

Third, we know that at the time the plasmoid begins to decay,

$$\omega_{ce} = 2\omega_{pe} \qquad \textbf{(4)}$$

,where ω_{pe} is the electron plasma frequency. This is due to the condition that when the synchrotron frequency exceeds twice the plasma frequency, energy can be radiated. At this point, the current begins to drop, and the change in the magnetic field sets up large accelerating potentials to sustain the current. This in turn generates the ion and electron beams that release the energy trapped in the plasmoid and initiate its decay, as well as start nuclear reactions. Finally, we assume that during compression the ratio B/n is a constant, as explained elsewhere [20].

From these basic physical relations, it is simple algebra to derive the plasma parameters in the plasmoid, not only for hydrogen, [20] but for any

gas or mixture of gases [21,23]. The results are summarized here:

$$r_c = 1.32\times10^{-3}(\mu\cdot z)^{-2/3} r \qquad \textbf{(5)}$$

$$B_c = 4z\left(\frac{\mu M}{m}\right)B \qquad \textbf{(6)}$$

$$n_c = 3.7\times10^{10}\,\frac{\mu^2 z I^2}{r^2} \qquad \textbf{(7)}$$

where B is peak field at cathode (G) , B_c is the field in the core of the plasmoid, r is cathode radius (cm) , r_c is the plasmoid core radius, n_c is plasmoid ion density, I is peak current (A), μ is average ionic mass and z is ionic charge.

The model [20] also allows us to describe the production of the electron and ion beams and the duration of the plasmoid. This is possible simply by equating the energy lost though the beams to the decay of the plasmoid B field. This allows the calculation of the accelerating potential, beam current and decay time.

$$\tau = 6.2\times10^{-6}\,\frac{r_c}{R_B} = 8.2\times10^{-9}\left(\frac{z}{\mu}\right)^{2/3}\frac{r}{R_B} \qquad \textbf{(8)}$$

$$n\tau = \frac{304\mu^{4/3} z^{1/3} I^2}{r R_B} \qquad \textbf{(9)}$$

Here, τ is plasmoid decay time, R_B is the effective resistance of the beam, n_c is plasmoid density. However, a modification must be imposed here. For low I and thus low accelerating potentials, all the particles in the plasmoid are evacuated through the beam without carrying all the energy away. In this case the simple model will break down near the end of the plasmoid decay. However, for present purposes a suitable approximation simply reduces the plasma lifetime by the ratio of the accelerating potential to that needed to carry the entire plasmoid energy. To a good approximation this factor turns out to be I/1.4MA. For I > 1.4MA, this factor is unity.

These theoretical predictions are in good agreement with results that were obtained experimentally in 2001 with a 1.2 MA DPF[22]. If we use these equations to predict B_c we obtain 0.43 GG, in excellent agreement with the observed value of 0.4 GG. Similarly, the formulae yield $n\tau = 4.6\text{x}10^{13}$ sec/cm^3 as compared with the best observed value in [22] of $9\text{x}10^{13}$ and the average of $0.9\text{x}10^{13}$.

For decaborane with Z = 2.66 and μ =5.166, with r = 5 cm, I =2.8MA these formulae yield B_c=11GG and $n\tau = 6\text{x}10^{15}$.

This is of course a considerable extrapolation—a factor of 60 above the observed values in both B and nτ. However, these conditions can be reached with relatively small plasma focus devices.

This is as far as the model in [20] takes us. We now turn to determining the fusion yield in the plasmoids, first elaborated in [21] but repeated here. It is clear that this yield is produced by two separate processes. In one process, the accelerated beam of ions collides with the background plasma in the plasmoid. In the second, the electron beam heats the electrons in the plasmoid, which in turn heat the ions, generating true thermonuclear fusion yield. The first is straightforward to calculate and gives the following result:

$$N' = 4\sigma(E_i) n_c \cdot r_c \cdot N_a = \frac{4\sigma(E_i) n_c \cdot r_c \cdot I_b \cdot \tau}{1.6\times10^{-19}} \qquad \textbf{(10)}$$

$$N' = \frac{2.96\times10^{18}\cdot\sigma(E_i)\cdot\mu\cdot I^3\cdot K}{R_B\cdot z} \qquad \textbf{(11)}$$

where N' is the neutron yield from the beam-plasma interaction. Here, again, K= $(\text{I}/1.4\text{x}10^6)$ does not exceed unity and $\sigma(E_i)$ is the reaction

cross section. Note that the beam interaction yield is not strongly affected by atomic number.

The question of heating is more complex. If the electrons simply collided with the plasmoid electrons through Coulomb interaction, heating would be quite inefficient. However, Heinrich Hora [27] has shown that, for a variety of plasma beam interactions, the electrons behave *as if* they have a cross section equal to a circle with radius equal to their Compton wavelength, hc/E rather the classical value of e^2/E. This of course increases the effective cross section by $1/\alpha^2$ or $2x10^4$. The reason for this relationship is not entirely clear. It occurs only in plasma, since the cross sections of electrons in gas are well known and correspond to the classical result.

Using the Hora formula for cross section of relativistic electrons, we can easily calculate the fraction of beam energy that goes into heating plasma electrons:

$$d_c = \frac{E_i^{\,2}}{\pi \cdot h^2 c^2 n_e} \qquad \textbf{(12)}$$

$$w = \frac{4r_c}{d_c} = \frac{3.92 \cdot \mu^{2/3} \cdot z^{2/3}}{r \cdot R_B^{\,2}} \qquad \textbf{(13)}$$

$$T_{e\max} = 721\left(\frac{z}{1+z}\right) keV \qquad \textbf{(14)}$$

$$T_{ef} = \frac{2.83\times10^6 \cdot \mu^{2/3} \cdot z^{5/3}}{r \cdot R_B^{\,2}(1+z)} \qquad \textbf{(15)}$$

Here, d_c is collision distance, w is the ratio of electron beam energy to heating energy, T_{emax} is the temperature for w=1. We take half the peak temperature as T_{ef}, the average electron temperature of the plasmoid, although this ignores the nonlinearity of reaction rate with T. We thus find that the temperature increases nearly as the cube of atomic number of the gas involved. Since $n\tau$ increases as $z^{2.4}$, the $n\tau T$ product increases as approximately z^5. We thus see the model's strong prediction of fusion yield improvement with increasing μ and z.

In general, the electron-ion heating time is small compared with the duration of the plasmoid:

$$t' = \frac{1.56\times10^7 \mu \cdot T_e^{3/2}}{n \cdot z^2} = \frac{4.2\times10^{-4} \cdot T_e^{3/2} \cdot r^2}{\mu \cdot z^3 \cdot I^2} \qquad \textbf{(16)}$$

$$\frac{t'}{\tau} = \frac{5.1\times10^4 \cdot T_e^{3/2} \cdot r \cdot R_B}{\mu^{-1/3} \cdot z^{7/3} \cdot I^2} \qquad \textbf{(17)}$$

We thus find the thermonuclear yield to be:

$$N = f(T_i) n^2 \tau 8\pi r_c^{\,3} = \frac{6.5\times10^5 \cdot \mu^{4/3} \cdot K \cdot I^4}{R_B \cdot z^{2/3}} f(T_i) \qquad \textbf{(18)}$$

where $f(T_i)$ is the reaction rate. The increase in $n\tau$ is partially countered by the decrease in the radius of the plasmoid and thus the total mass involved, so exclusive of the increase in T, yield increases only as $z^{1.4}$, assuming a constant μ/z. But the strong increase in T generates an even sharper rise in yield. Since T increase with decreasing r, up to the point w=1, smaller cathodes increase yield as well.

It should be noted that the thermonuclear yield , which should be observed as isotropic, scales as I^4 while the beam-plasma yield observed as anisotropic scales as I^3, so the degree of anisotropy will decrease with increasing current and total yield.

5. Control of Angular Momentum and Efficiency of Energy Transfer to the Plasmoid

The appropriate choice of cathode radius, peak current and fill pressure is not enough to ensure the efficient formation of a plasmoid that contains the full magnetic energy input to the device. In fact, in few of the existing DPF devices is the efficiency of energy transfer into the plasmoid very high, limiting yield to well below that predicted by the model described in the section "Conditions of DPF Plasmoids". For high efficiency, control of angular momentum is required, as first pointed out by Lerner and Blake [23].

The process of plasmoid formation involves the development of a kink instability in the current flow at the pinch and as such requires a certain amount of angular momentum. We here refer to total angular momentum, both of the magnetic field and of the particles. Another way of looking at this is that the axial field/ azimuthal field ratio has to be sufficient for the kinking to occur. During the compression phase, angular momentum per unit mass is conserved, so this angular momentum can be derived from angular momentum present in the filament array at the time the compression begins. An approximate measure of the angular momentum per unit mass required can be obtained by the formula $0.5\ V_A r$, here V_A is the Alfven's velocity in the plasmoid and r is the plasmoid radius.

Angular momentum can be imparted to the plasma sheath during the rundown by the interaction of the inward flowing electron flows and any small initial axial magnetic field (e.g., the small axial component of the earth's magnetic field). The JXB force accelerates the electrons slightly in the azimuthal direction, creating an azimuthal component to the current. This in turn increases the axial magnetic field and thus the azimuthal acceleration of the electrons. In this way, a very small initial magnetic field (or small, random initial azimuthal component in the current created by irregularities in the electrodes) can be rapidly magnified. For example, given a ratio of axial to total magnetic field $B_\theta/B_T=\sin\theta$ then any initial axial field will be amplified so that at the end of the run down $\theta= \theta_i e^{V\tau/R}$, where τ is the run down time and R is the anode radius. Thus final angular momentum per unit mass is $VR\ \theta_i e^{V\tau/R}$ where V is the Alfven velocity at the anode radius at peak current.. This is a simplified analysis, as in the real case B_T is rising rapidly during the early stages of the pulse. However, a numerical analysis using a realistic function for B_T shows a very similar result, as at later times, the magnitude of the initial axial field is very small compared with B_T, so the amplified field dominates, as in the simplified formula.

Since $V\tau/r$ is proportional to L/R, the angular momentum is sensitively dependent on this ratio. If there is insufficient angular momentum, the plasmoid radius will be reduced in proportion to angular momentum and the total plasmoid energy and mass will be reduced as the cube of angular momentum. This sensitivity to initial very small angular momentum can in part explain the well-known shot-to-shot variability of plasma focus devices. Calculations show that if this natural amplification mechanism is relied on to provide angular momentum and the initial magnetic field is the earth's ambient field, L/R must be more than about 7 for high efficiency of energy transfer into the plasmoid. Indeed, in the best-performing DPF devices, this ratio exceeds 7 and can be as high as 17, implying that high V_A and longer τ are desirable.

The disadvantage of such long electrodes is their high inductance, around 20 nH. Since external inductance must exceed load inductance, total inductance in the system must be around about 45 nH. As Lee [28] has shown, these considerations lead to limitations on the total amount of current that can be fed into the DPF from a capacitor

bank, as the pulse length must increase as capacitance does, unless the charging voltage becomes very high. The high inductance, by forcing up total bank energy, reduces the proportion of that energy that can be converted into the DPF magnetic field. So even if the efficiency of energy transfer from the magnetic field to the plasmoid increases, the total efficiency from capacitor bank to plasmoid does not necessarily increase.

The alternative to relying on amplification of the ambient magnetic field, is to inject angular momentum with a small artificial axial magnetic field, produced by a helical coil. While there have been previous efforts to stabilize DPF pinches with axial fields, these fields have been much greater than those contemplated here, generally thousands of G. If the model described here is valid, too much angular momentum will prevent the plasmoid from being formed and thus drastically reduce fusion yield. Only the optimal amount of field, of the order of a few G, will provide enough angular momentum to just balance the compressional pinch forces and form the largest possible plasmoid.

Viewed in another way, for a given electrode radius and length, the injection of angular momentum will greatly increase the angular momentum and thus the size of the plasmoid, and thus the energy yield from fusion reactions in the plasmoid. Approximately, fusion yield will increase as the third power of the amount of injected angular momentum.

6. Experiments with Focus Fusion-1

To test the above mentioned, and other theoretical predictions, we have constructed a new DPF facility (called Focus Fusion-1, or FF-1 for short) in Middlesex NJ, with a 113μF, 45 kV capacitor bank, which we expect will be able to achieve peak currents above 2MA.

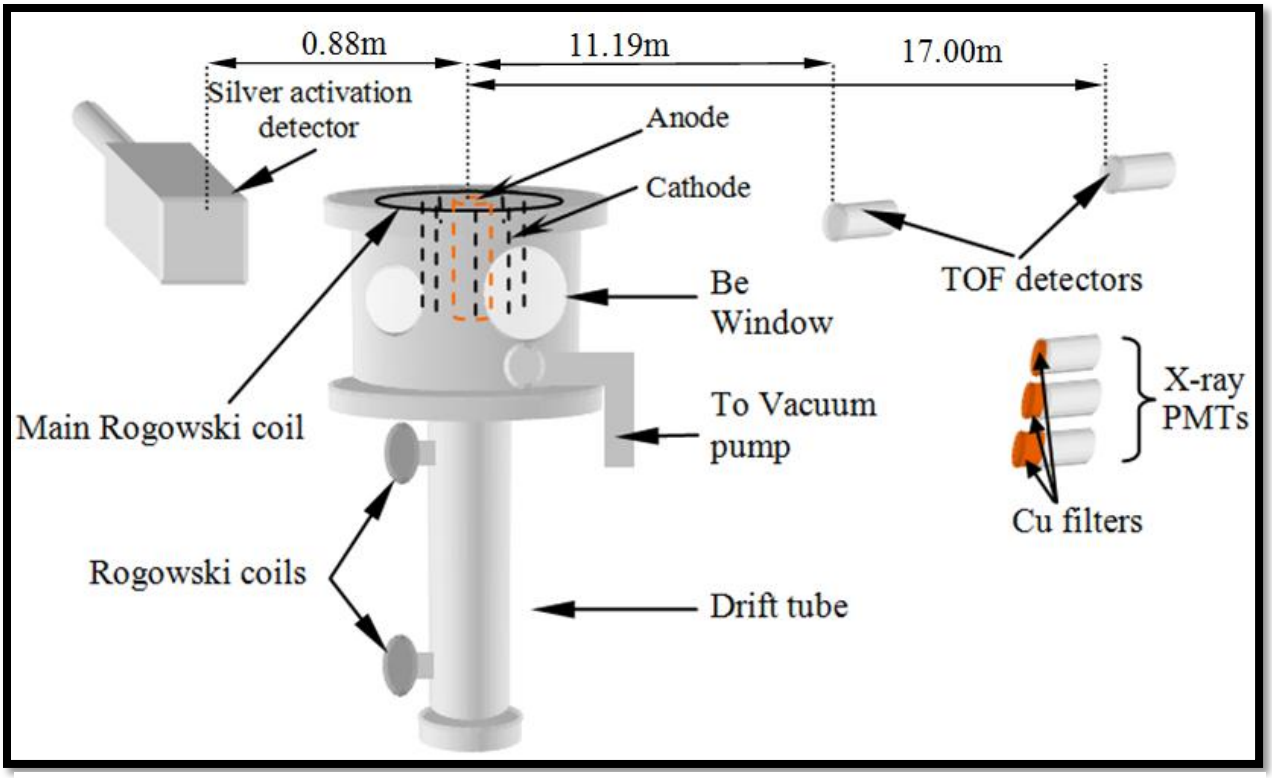

Figure 1. Experimental setup of Focus Fusion-1

The design of FF-1 is based on the accumulated experience of the DPF field but represents an advance in two major ways. First, we expect that it will achieve a very high current with a very compact and relatively economical design by achieving a low external inductance of about 15 nH. With a capacitor bank total capacitance of 113 microfarads and a maximum charge potential of 45kV, we expect the device to achieve a peak current of 2.2 MA using deuterium with 14-cm long anodes and as high as 2.8 MA using heavier gases and shorter anodes. Exclusive of the support structure, the entire device fits in a 2.5x2.5x1 meter volume. Second, for these high peak currents, FF-1 has very compact electrodes, thus generating a high initial magnetic field. The cathode consists of 16 copper rods set at a radius of 5 cm and the anode is a hollow copper cylinder 2.8 cm in radius. At the highest peak current, the field at the anode surface will be around 200 kG, which we estimate is close to the highest field allowed by the mechanical strength of copper. These high fields will make possible high fill gas densities, which in turn will lead to high final densities in the plasmoids. Six different anodes ranging in length from 7-14 cm will be used, depending on the fill gas.

Figure 1 illustrates the vacuum chamber and the drift tube arrangement. The vacuum vessel is made of stainless steel SS304 with internal dimensions of 10 cm diameter and 30 cm height. It has been annealed to prevent it from acquiring a permanent magnetization, and thus complicating the axial field experiments. The drift tube is 100 cm long. A copper coil generates the axial B-field necessary for angular momentum injection. A knife edge consisting of 100 tungsten pins is placed around the anode close to the insulator and promotes the formation of filaments. The insulator is made of alumina ceramic. The chamber is initially evacuated using a Pieffer turbomolecular pump to ultra high vacuum levels. After this pump down, the deuterium gas is flowed into the chamber until the predetermined pressure is reached.

The experiment currently uses 13 diagnostic instruments to measure the various parameters of the plasma and the tiny plasmoid. We have listed the instruments by the parameter they are designed to measure. To measure the size and shape of the plasmoids we use:

A 4PICOS Stanford Computer Optics ICCD camera with 0.2 ns minimum exposure time. The ICCD is sensitive to UV radiation down to 180 nm and thus should be able to observe radiation above the plasma frequency of the plasmoids for all deuterium experiments, although not for the heavier gases. In addition to its high temporal resolution, the ICCD currently has a spatial resolution of about 30 microns. We also use an x-ray pinhole camera.

To measure the electron energy distribution we use:

A set of three scintillators and PMT x-ray detectors each located behind a different thickness of copper filter—300 microns, 3mm, 6 mm. The ratios of the signals from the PMTs measure the average x-ray emission and can be fitted to a model of bremmstralung radiation to obtain the average electron energy with high time resolution. The detectors are shielded by a 5cm lead brick from the emissions due to the collision of the electron beam and the anode, so that we are measuring x-rays from the plasmoids alone. The detectors are also shielded by copper sheaths from the RF pulse which arrives at the same time as the x-ray pulse.

The energy of the ions is measured by two neutron time of flight (TOF) detectors that consist of two scintillation detectors with PMTs placed at different distances –11 meters for the near detector and 17 meters for the far detector. The difference in the detection times of the two detectors measures the energies of the neutrons,

thus allowing us to differentiate between the 14.7 Mev and 2.5 Mev neutrons from the D-T and D-D reactions. In addition, the spread in energies, indicated by the widening of the pulse with distance, gives us a measure of the ion velocities within the plasma. Since x-rays arrive first at the detectors, they produce a distinct signature and can be easily isolated from the neutron signal.

The TOF detectors can also be used to determine the density of the plasmoid. Since the DT neutrons can only be produced from tritium that is itself generated by DD reaction within the plasmoid, the ratio of DT to DD neutrons gives a direct measurement of the density of the plasmoid. In addition, if we know the volume of plasmoid from the pin whole camera, ICCD camera and the X-ray lens, and we know the electron temperature from the x-ray spectrometer, we can put these values together with a standard formula from the total amount of X-rays. We can then determine density using formula:

$$P_x = 1.6 \times 10^{-32} n_i^{\,2} \cdot V \cdot T_e^{\,1/2} \qquad \textbf{(19)}$$

Where P_x is total x-ray power. The average ion energy can also be cross-checked given the density and volume of the plasmoid by the formula

$$N = n_i^{\,2} V \tau < \sigma v > \qquad \textbf{(20)}$$

Where '*N*' is neutron yield, '*V*' is the volume, τ is confinement time, $<\sigma v>$ is the reaction cross-section, n_i is the ion density In this manner every plasma parameter is obtained by at least two independent means and in most cases three.

Neutron measurements are made with two BTI bubble detectors, each calibrated by the manufacturer to +_25%. In addition, we have built a silver activation detector exactly following a previously calibrated design. [29]. We have cross-calibrated the neutron detector with the bubble detectors and find them in agreement within 10%.

The ion beams are measured with two Rogowski coils built into the drift tube, one at 30 cm from the end of the anode, the other at 100 cm. The coils provide a measure of both the net current of the beams, and by time-of-flight calculations the energy distribution of the ions.

A main Rogowski coil built into the lower (ground) base plate records the dI/dt of the current through the anode and is integrated digitally to provide the current measurement. We have calibrated the current to within 5% by comparing the integrated current with a waveform generated by a detailed run-down simulation developed by Lee [28] for the measured capacitance, charging voltage and other characteristics of our device. The resulting calibration is also within 5% of that calculated from the inductance of the coil.

Finally, a HV probe measures the voltage on an individual spark plug.

7. Preliminary experimental results.

So far, we have fired FF-1 over 500 times since it produced its first pinch on October 15, 2009. We have been somewhat slowed by the poor initial functioning of the switches, supplied by R. E. Beverly and Associates, which required extensive modification and rebuilding. However, we report here on some important preliminary observations which will be elaborated in future papers.

First, the fusion yield, as measured by the silver activation detector, depends sensitively on the time of the pinch. Much other DPF work has shown that the highest yields are obtained when the pinch occurs close to the quarter-cycle time of the device, when the maximum current would occur without the pinch. Here we define the pinch time as the time at which dI/dt has a minimum and thus the rate of energy transfer into the plasmoid is at a maximum. However, most researchers have found that the actual peak in yield occurs with a pinch time somewhat later than the quarter-cycle time, when the current is actually decreasing [30].

This is true for our FF-1 results as well, *but only if the axial magnetic field is absent.* When the field is present, we find that fusion yield increases significantly—by more than a factor of three—when the pinch time is exactly at the quarter cycle time (within ±3%).

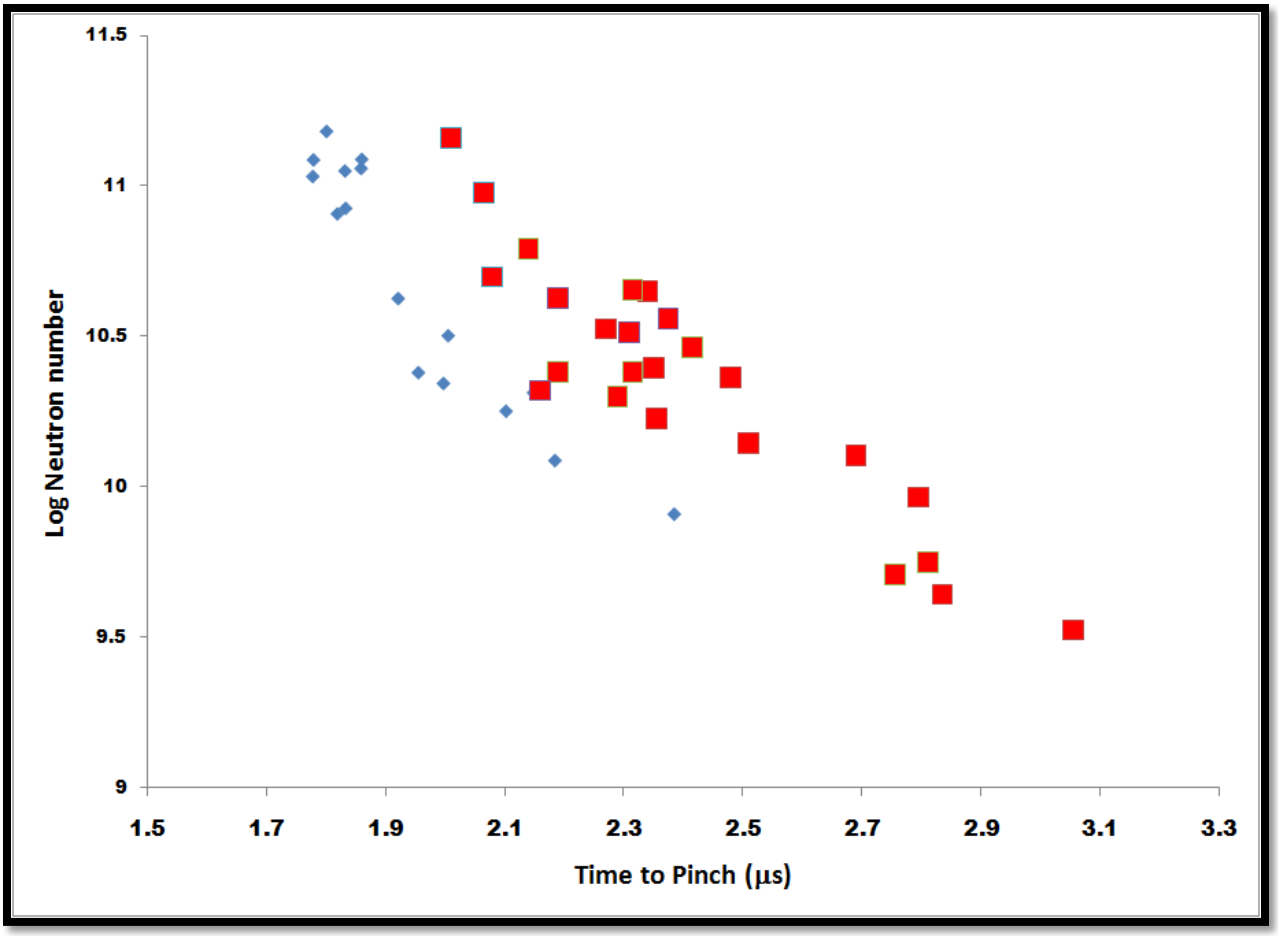

Figure 2. Log neutron yield vs time to pinch. The small dots are shots at 10 torr fill pressure while the large ones are at 18-24 torr. Error bars are omitted for clarity and are 0.1 for log yield and extremely small—less than 5 ns—for time. Quarter-cycle time is 1.8 µs.

As shown in figure **2**, the results for shots at 10 torr D fill pressure tightly follow a steep scaling curve**.** All of the shots with the highest yield, and with pinch times between 1.78 and 1.86 microseconds—very close to the quarter-cycle time of 1.8 microseconds—were obtained with an additional axial field. In these particular cases, the field was about 1 gauss and was imposed by the magnetization of the vacuum chamber before we annealed the chamber to prevent such magnetization. No shots without the imposed axial magnetic field have such high yields or short pinch times. For those shots, the maximum yield occurs with pinch times >2.0 µs (thus for R>1.1, where R is the ratio of pinch time to quarter-cycle time). The peak current in these shots varied between 630 kA and 720 kA.

The shots taken at higher current (around 1 MA) and with fill pressures of 18-24 torr show the same pattern, but with an increase in yield of about a factor of 4-5 at the same pinch times. This shot series demonstrated that the short-pinch time regime was not accessible without the additional axial field. Without this imposed field, when the

fill pressure was reduced sufficiently for rapid run-downs and thus short pinch times, no pinch occurred.

An indication of the physical processes associated with these different yields is provided by the main Rogowski coil traces, which record the dI/dt of the current passing through the anode. For the long-pinch-time pulses (LPTs), those with R>1.1, the characteristic fall in dI/dt at the time of the pinch is not smooth, but is interrupted by one or two large bumps, where the decline in current, and thus the transfer of energy into the plasmoid, is interrupted (Figure 3). This phenomenon occurs in all the LPTs that we have observed.

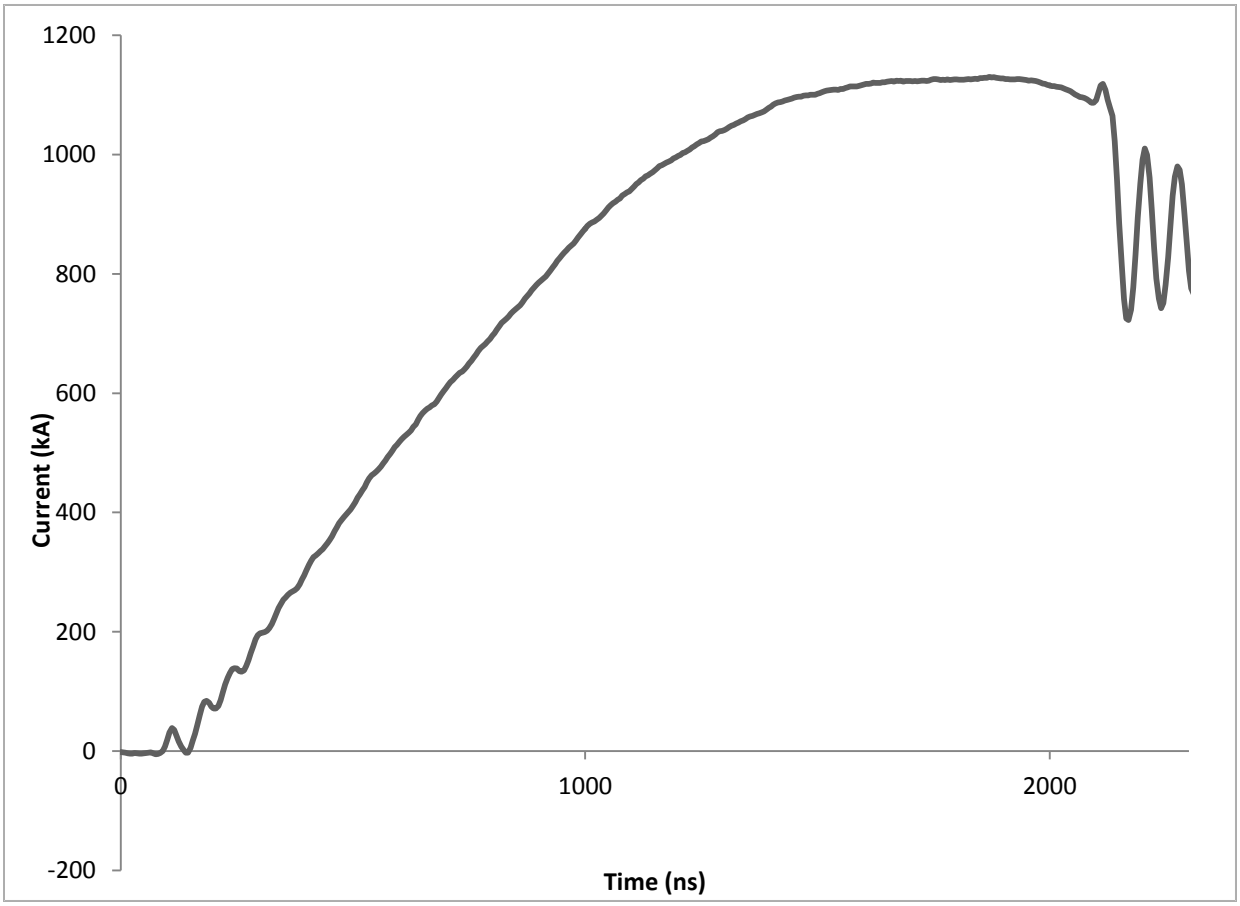

Figure 3. Current vs time, shot 10011002, an LPT, with pinch process starting with negative dI/dt. Note the small bump in current before the pinch.

By contrast, all of the short-pinch time pulses (SPTs) have smooth decreases to the pinch. (Figure 4) and smooth increases in voltage.

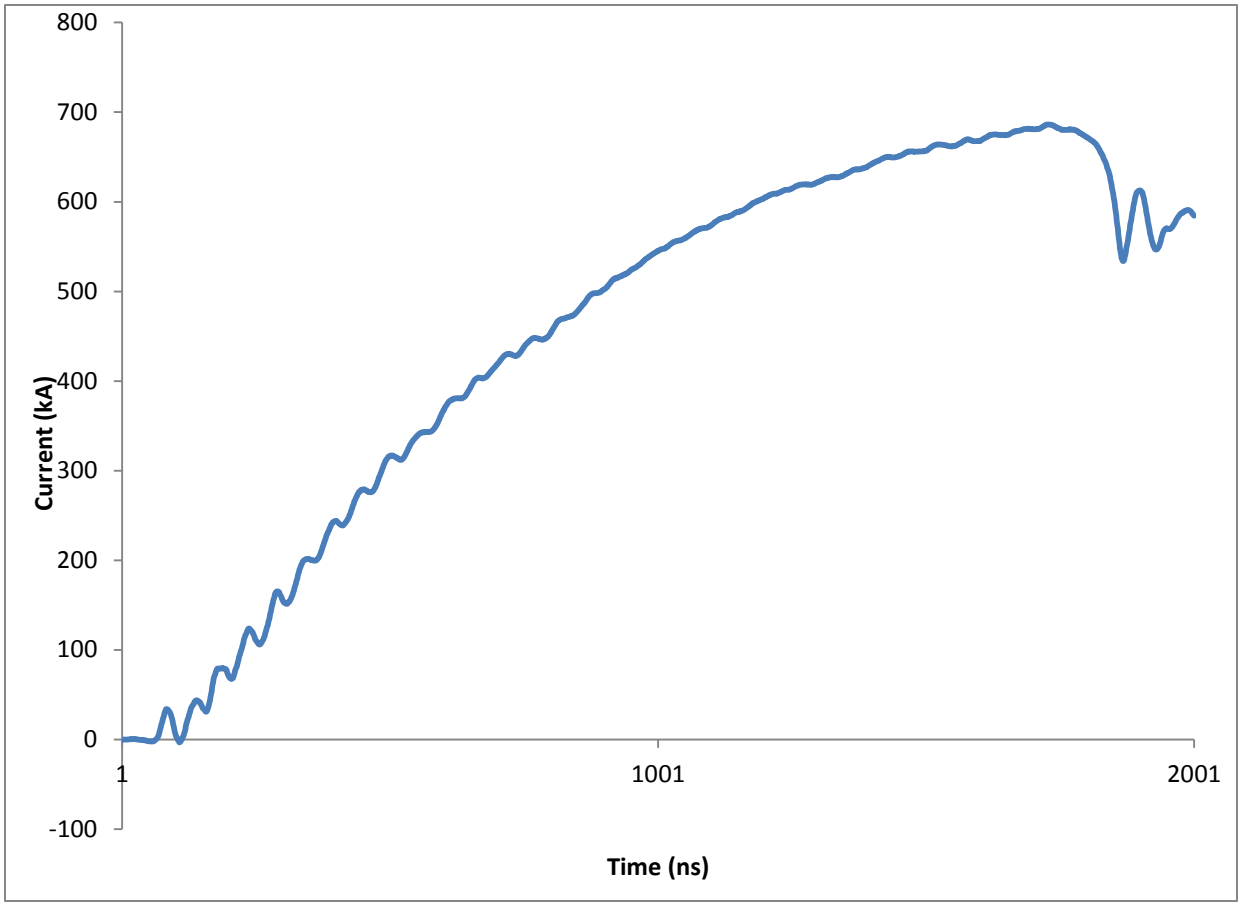

Figure 4. Current vs time, shot 03301010, a SPT with pinch process starting with positive dI/dt. Note the smooth decline in current into the pinch.

The bumps characteristically precede the pinch maximum by only 30-50 ns. At this time, the current sheath has already converged onto the axis of the anode. We know this from our ICCD images, which show that the sheath is on the axis as early as 225 ns before the pinch (fig.5). So whatever physical process are causing the bumps, occur in the final stages of the formation of the plasmoid.

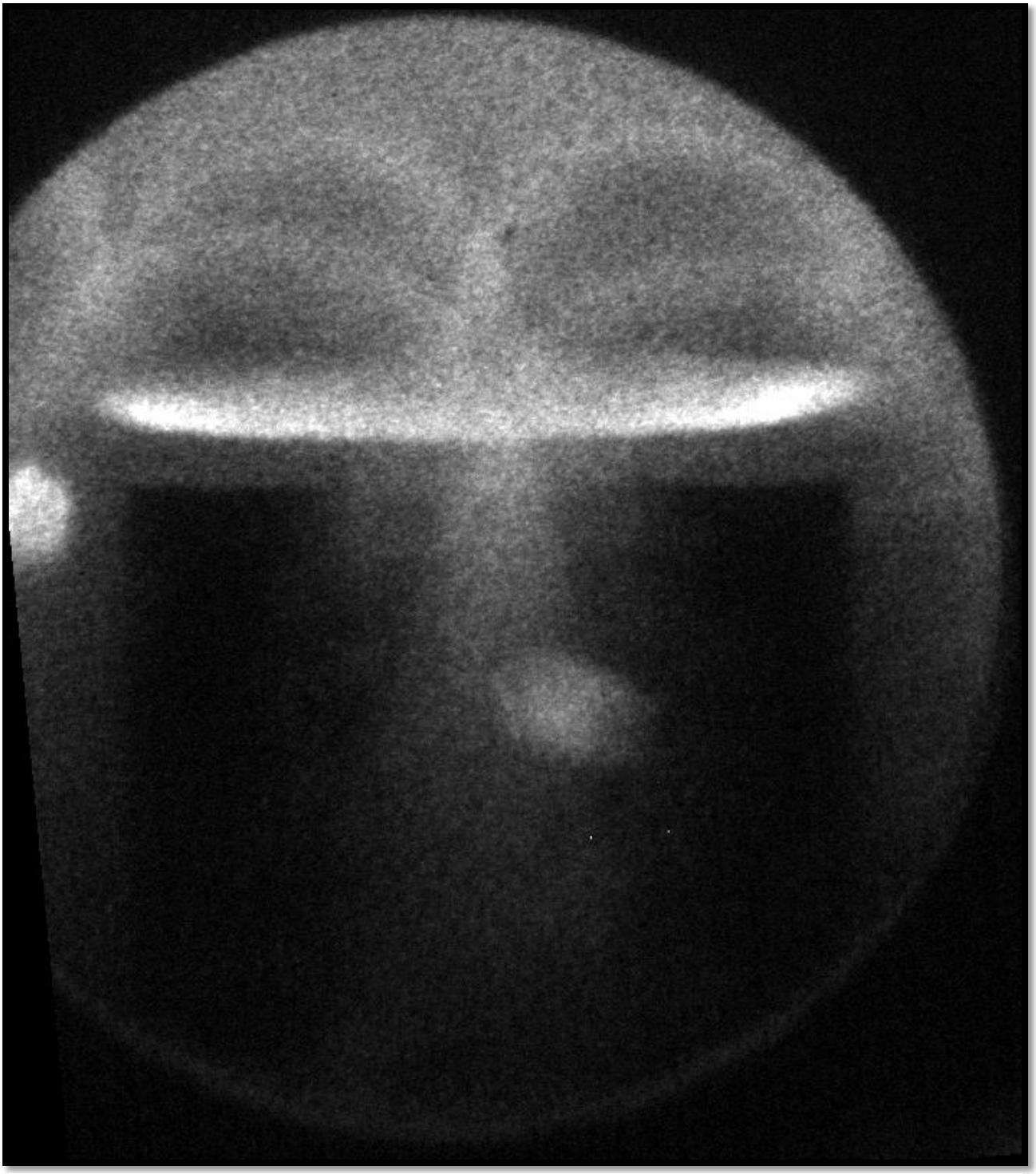

Figure 5. ICCD image of end of anode at 225 ns before pinch, exposure time 0.2 ns. Note the convergence of the filaments at this time on the axis of the anode. The circle is the viewing window and the bright horizontal ellipse is the hole in the anode.

It is significant that the yields of the STPs exceed those obtained by other DPFs at the same current by about a factor of six (figure 6). Thus, the best yields obtained without the additional axial field are comparable to those obtained elsewhere, but the STPs obtained with the axial field have considerably higher yields than the historical DPF trend.

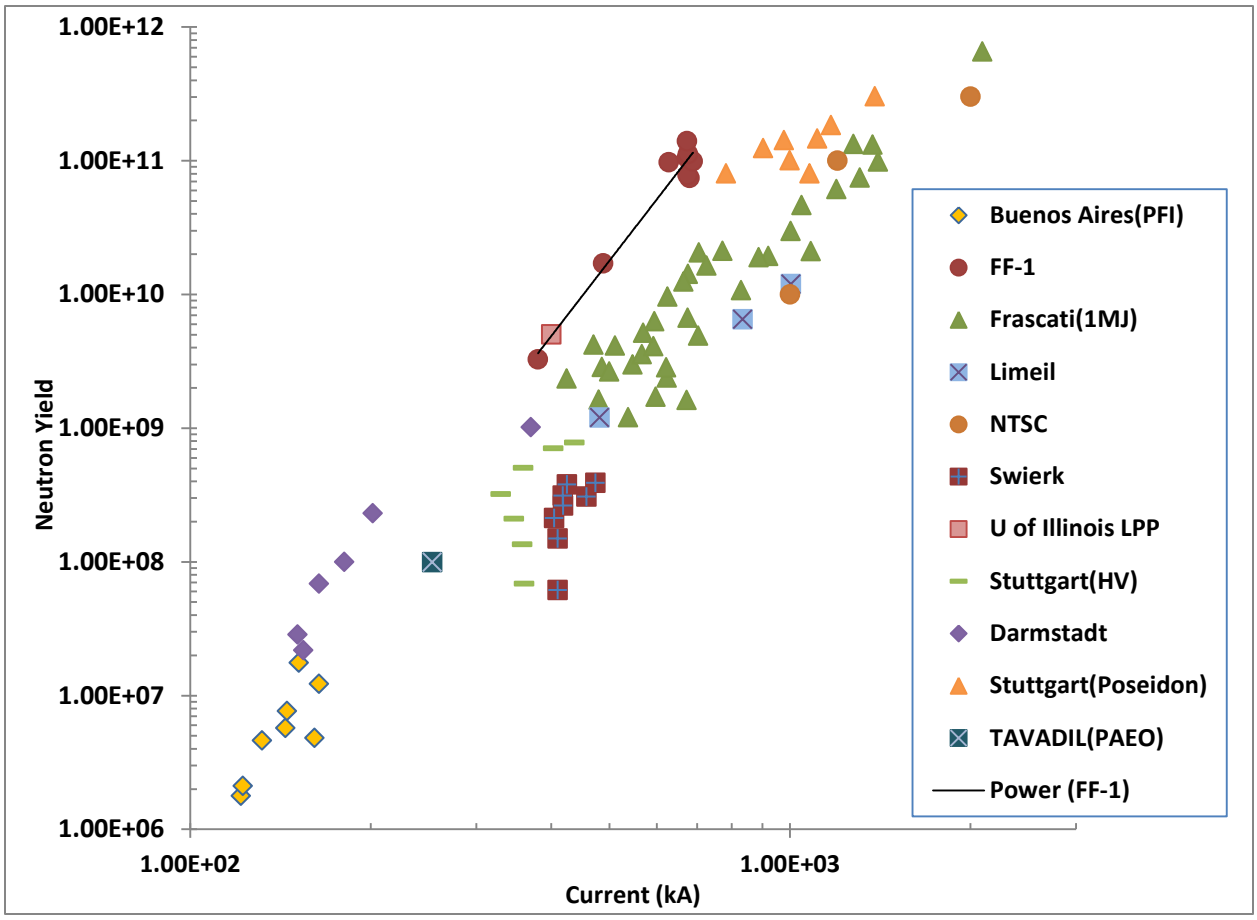

Figure 6. FF-1 SPT results, filled circles on line, fall above the historic trend line of DPF results. Data is from M. Milanese and J. Pouzo [31], except for U of Illinois and FF-1. Line is power-law fit to FF-1 data.

8. Comparison with theory and tentative explanation of results

We can compare these preliminary results with the yield predicted by the theoretical model described in this paper. Equations 11,15 and 18 enable us to calculate a predicted yield based only on the peak current and the cathode radius of the device. Table 1 shows a comparison of the predicted yield with those actually observed for the STPs. As can be seen there is good agreement with these yield observations. We are in the process of comparing the other predictions of the model with observations.

Our results pose a number of questions that we can provide only tentative answers to at this time. Why are the yields much higher for the STPs than for the LTPs? Why are the STPs obtainable only with the imposed axial field? What is the significance of the bumps in the dI/dt?

It is reasonable to hypothesize that the two precursor bumps are caused by shocks which heat the plasma before the plasmoid is fully compressed, decreasing the amount of energy available for the plasmoid and possibly as well the amount of angular momentum. One likely time for such shocks to occur is in the final stages of the kinking process, when the coils of the kinking filament are approaching each other at high velocity. It is possible that with adequate injected angular momentum, due to the increased axial field, these shocks will be greatly decreased, as the coils will slide past each other in a spiral fashion, rather than colliding head-on. This would allow greater energy transfer other plasmoid and thus the higher yields. Of course, such a conclusion requires a good deal more evidence to be validated.

We note that, as described in the section "Control of Angular Momentum and Efficiency of Energy Transfer to the Plasmoid", the angular momentum is increasing exponentially with time. If a minimum amount is essential for the formation of the plasmoid, and thus for the pinch, the time needed to reach this minimum will be reduced if the initial axial field is greater. So an alternative explanation of the role of the axial field is that it allows this minimum to be reached before the pinch time, thus allowing the SPTs to take place.

The role of the precise timing of the pinch is less clear. Since the shocks occur before the pinch and presumably determine the energy transferred, the

Shot #	***Fill pressure (torr)***	***peak I (kA)***	***$Yield_{obs}$ ($x\ 10^{11}$)***	***$Yield_{pred}$ ($x\ 10^{11}$)***	***$\frac{Pred}{Obs}$***
33003	10	674	1.05	1.54	1.45
33004	10	680	0.74	1.63	2.18
33005	10	675	0.77	1.55	1.99
33006	10	689	0.99	1.78	1.79
33007	10	627	1.03	0.94	0.9
33009	10	676	1.13	1.56	1.39
33010	10	674	1.4	1.53	1.09
31202	10	720	1.13	2.39	2.11
70605	7	488	0.2	0.167	0.83

Table 1. Comparison of Observed and Predicted Yield, SPTs

critical periods would logically be *before* the shocks, when the rapid fall in dI/dt just begins (in our hypothesis, with the start of the kinking process). In that case, the start of this fall in dI/dt occurs when the current is *rising* for all of the STPs and when it is *falling* or near zero for all of the LTPs. To be precise, all the STPs have dI/dt $>10^{11}$ A/s at the time the pinch begins—a sudden shift to high negative dI/dt--while all the LTPs have dI/dt $<3x10^{10}$A/s at this time and the vast majority have dI/dt <0. So the sign of dI/dt seems to be highly significant as well as its magnitude. The question then arises: why does the sign of dI/dt affect the shock process and how does it interact with the imposed axial field?

Tsybenko and Miklaszewkis [32] looked at the problem of pinch timing based on the observation that, in most DPFs, the maximum yields are slightly after the quarter cycle time. They hypothesized that a tangential discontinuity, which occurs when two adjacent parts of a cylindrical plasma are rotating at different frequencies, could set off instabilities that disrupt the pinch. They show that such an instability is suppressed if the current in the column is varying at a frequency comparable to the instability growth time—around 10 ns. However, in our observations the current varies over a time scale of 6-7 microseconds, so it is hard to see how this mechanism could be significant.

It is possible that the azimuthal potential induced by the dI/dt can add to or subtract from the angular momentum provided by the axial field coil to produce the optimal amount of angular momentum both for minimizing the shocks and forming the plasmoid, but at the moment a complete explanation of the data is not yet in hand. We expect that experiments now underway will greatly clarify the outstanding theoretical questions.

Acknowledgement: The authors wish to thank John Thompson for his major contributions to the design and construction of FF-1.

References

1. C.L. Leakeas, "Parameteric studies of dense plasma focus for engineering space propulsion" (P1-TR-91-3014, Phillips Laboratory, AFSC, 1991).

2. C.C.Choi, , "Engineering considerations for the self-energizing MPD-type fusion plasma thruster", (PL-TR-91-3087, Phillips Laboratory, AFSC, 1992).

3. G.H. Miley, et al, "Use of a plasma focus device for space propulsion," *Advanced SEI Technologies Conference,* AIAA-91-3617 (1991).

4. W.H. Bostick, et al, *Ann. NY Acad. Sci.*, 251, 2 (1975).

5. C.R.Haas, et al, "Dynamics of Microstructures," *Proc. 3rd Int. Workshop on Plasma Focus*, p.87 (1984).

6. G. Herziger, et al, "Radiation and particle emission from a 1.6kJ plasma focus", *Proceed. Int. Conf on Plasma Physics*, Lausanne, July2-3, 1984, p.31 (Ecole polytechnique federal de Lausanne,1984)

7. H. Schmidt, et al, Ion and neutron emission of the Poseidon plasma focus, Proc 3rd Int Workshop on Plasma Focus, p. 63-66 (1984).

8. K. N. Koshelev et al, *J. Phys D*, 21, 1827 (1988).

9. W .Bostick, V. Nardi, W. Pryor, *J. Plasma Phys* 8, 7 (1973)

10. M. Sadowski et al, *Phys. Lett*, 105 A, 117 (1984)

11. L. Bertalot et al, "Experiments on plasma focus dynamics, neutron production and ion

emission," IAEA Plasma Physics and Controlled Nuclear Fusion, International Conference, Brussels, July 1-10, 1980, p. 177 (IAEA, Vienna,1980).

12. J.S. Brzosko, et al, *Physics Letter A*, 192, 250 (1994)

13. J.S. Brzosko, et al, *Phys. Plasmas* 2, 1259 (1995)

14. G.R.Neil, R.S. Post, *Plasma Phys.*, 14, 425 (1988).

15. I.Volobuev et al, Sov. J., *Plasma Phys.*, 14, 401 (1988).

16. K. Hirano, et al, "Plasma dynamics and charged particle emission in the plasma focus," *Proc. 11th Europe Conf. Controlled Fusion and Plasma Physics* Aachen, Sept.5-9, 1983 1, p. 551 (European Physics Society, Geneva,1983).

17. L. Jakubowski, M. Sadowski, J. Zebrowksi, *Nuclear Fusion*, 41, 755 (2001)

18. L. Bertalot et al, *Phys. Lett A*, 79 389 (1980)

19. V.Nardi, et al, *Phys. Rev.*, A22, p. 2211 (1984).

20. E.J. Lerner, *Laser and Particle Beams*, 4, Pt. 2, 193(1986)

21. E.J.Lerner, A.L Peratt, Final Report, Jet Propulsion Laboratory contract 959962 (1995).

22. E. J. Lerner, in *Current Trends in International Fusion Research—Proceedings of the Fifth Symposiu*m, Edited by E. Panarella, NRC Research Press, National Research Council of Canada, Ottawa, ON K1A 0R6 Canada, (2007).

23. Method and apparatus for producing x-rays, ion beams and nuclear fusion energy US Patent # 7,482,607

24. E. J. Lerner, R. E. Terry, *Current Trends in International Fusion Research—Proceedings of the Sixth Symposium*, National Research Council of Canada, 2009, pp11-22.

25 J.R. McNally, *Nucl. Fusion*, 15, 344 (1975

26. G. S. Miller, E.E. Salpeter, and I. Wasserman, *ApJ*, 314, 215 (1987)

27. H. Hora, . *Plasmas at High Temperature and Density*. Section 2.6 Heidelberg: Springer 1991

28. S.Lee, *Applied Phyiscs Letter* 92, 021503 _2008

29. D. R. Slaughter and W. L. Pickles, *Nucl Instrum Methods*, 160 (1979) 87-92.

30. VA Gribkov, et al *Trudy FIAN*, 127:32 (in Russian) . (1980)

31. M. Milanese and J. Pouzo, Small Plasma Physics Experiments, World Scientific Publishing, London, 66 (1988)

32. S. P. Tsybenko, R. Miklaszewski, *NUKLEONIKA*;45,163 (2000)